NANO-MICRO LETTERS ARTICLE
www.nmletters.org

Shape-controlled Synthesis of Porous SnO_2 Nanostructures via Morphologically Conserved Transformation from SnC_2O_4 Precursor Approach

Qihua Wang[1], Dewei Wang*[,1,2], Tingmei Wang[1]

(Received 18 Feb 2011; accepted 08 April 2011; published online 19 April 2011.)

Abstract: Porous SnO_2 nanostructures with controlled shapes were synthesized by a facile morphologically conserved transformation from SnC_2O_4 precursor approach. Well-defined SnC_2O_4 nanostructures can be obtained through a solution-based precipitation process at ambient conditions without any surfactant. The formation mechanism of such microstructures was tentatively proposed on the basis of intrinsic crystal structure and the reaction conditions. We found that the morphologies of precursor were well maintained while numerous pores were formed during the annealing process. The combined techniques of X-ray diffraction, nitrogen absorption–desorption, field emission scanning electron microscopy, and (high-resolution) transmission electron microscopy were used to characterize the as-prepared SnO_2 products. Moreover, cyclic voltammetry (CV) study shows that the shape of CV presents a current response like roughly rectangular mirror images with respect to the zero-current line without obvious redox peaks, which indicating an ideal capacitive behavior of the SnO_2 electrodes. The photoluminescence (PL) spectrum study suggests that the as-obtained porous SnO_2 nanostructures might have a large number of defects, vacancies of oxygen, and local lattice disorder at the interface, interior and exterior surfaces.

Keywords: Shape-controlled; SnO_2; Solution chemistry.

Citation: Qihua Wang, Dewei Wang, Tingmei Wang, "Shape-controlled Synthesis of Porous SnO_2 Nanostructures via Morphologically Conserved Transformation from SnC_2O_4 Precursor Approach", Nano-Micro Lett. 3 (1), 34-42 (2011). http://dx.doi.org/10.3786/nml.v3i1.p34-42

Introduction

As one of the versatile functional materials with a stable wide band gap of 3.6 eV, SnO_2 has drawn immense attention to its fascinating physicochemical properties and potential applications in numerous fields, such as transparent conductive electrodes, anodes for lithium ion batteries, dye-sensitized solar cells, and chemical gas sensors [1-4]. Recent studies show that the performance of SnO_2 in these applications mainly depend on its morphology and structural features. Accordingly, considerable effort has recently been devoted to synthesizing SnO_2 nanostructures with different morphologies, including SnO_2 octahedra, nanorods, nanowires, nanobelts, nanotubes, hollow spheres, and mesoporous structures [5-15]. Particularly, nanoporous structures have attracted considerable attention due to their improved performance compared with their solid counterpart, such as large surface area, efficient catalytic activity, and structural stability [16]. It is believed that

[1]State Key Laboratory of Solid Lubrication, Lanzhou Institute of Chemical Physics, Chinese Academy of Sciences, Lanzhou, 730000, People's Republic of China.
[2]Graduate School of Chinese Academy of Sciences, Beijing, 10039, People's Republic of China.
*Corresponding author. Fax: +86-931-8277088; Tel: +86-931-4968180; E-mail: wangqh@lzb.ac.cn, wangdewei@yeah.net.

nanoporous structures with controllable shapes might allow us to harvest advantages of both morphology and porous structure, which could widen their applications.

Typically, the template-assisted approach has been demonstrated to be an effective route that can be employed to produce porous SnO_2 nanostructures. For example, mesoporous SnO_2 has been synthesized through structure replication (nanocasting) from ordered mesoporous KIT-6 silica by Tiemann and co-workers [17]. Qi and co-workers employed 1D silica mesostructures as sacrificial templates to synthesize SnO_2 nanotubes with preserved morphologies via a simple hydrothermal route [18]. Highly ordered mesostructures of SnO_2 have been obtained via an evaporation-induced self-assembly process [19]. However, to obtain pure porous materials, these template strategies encompass the need to remove the template through calcinations at elevated temperatures or wet chemical etching with an appropriate solvent. In some cases, the pore structure would be destroyed or the wall has poor mechanical strength during the template removal process. Moreover, template contamination mostly decreases the activity of synthesized materials and the removal of residues is difficult, which limit their performance [20]. Furthermore, the morphologies of the porous structures are limited due to the difficulty in fabricating templates with diverse morphologies. Therefore, the development of cost-effective methods, suitable for the large-scale synthesis of SnO_2 nanoporous structures with adjustable morphologies, remains to be a huge challenge.

Recently, morphology conversion transformed from precursor route has been explored to generate other nanostructures that might be difficult to synthesize directly. For instance, Xia and co-workers have demonstrated that the porous SnO_2 nanowires can be obtained by calcination nanowires precursor, which has been prepared by reflux in the polyalcohol medium at a high temperatures [21]. SnS_2 also could be serving as a precursor to generating porous SnO_2 nanostructures with preserved morphologies via a simple calcination process [22]. Tin oxalate can be used as an alternatively precursor which can be producing SnO_2 due to their easy synthesis, low cost, good structure stability, and relatively low decomposition temperature in air [23]. For example, tin oxalate submicrotubes, nanorods, and flowers-like structures can be obtained in the presence or absence of the surfactant. Porous SnO_2 nanostructures can be obtained after calcination tin oxalate precursor at the relatively high temperatures (typically 500℃) in air [24-27]. Despite these advantages, it is still a great challenge to synthesize tin oxalate nanostructures in high quality in terms of well-defined shape and ease of fabrication. Herein, we report a simple but effective approach for producing mesoporous SnO_2 nanostructures via a two step process. SnC_2O_4 with three distinct morphologies, i.e., microfibers, nanorod-bundles and sheaflike shape, have been successfully synthesized via a solution-based precipitation process in a selective manner. We found that the shapes of the tin oxalate could be tuning just through simply altering the solvents used. During heating at 350℃ in air, SnC_2O_4 undergoes a transformation to SnO_2 without altering the morphology of their respective precursors. This facile efficient and economic work provides a new route to synthesize mesoporous SnO_2 nanostructures with controllable shape.

Experimental

Synthesis of SnC_2O_4 microfibers: In a typical procedure, 1 mmol of oxalic acid ($H_2C_2O_4$) and an equal mole ratio of tin chloride dihydrate ($SnCl_2 \cdot 2H_2O$) were first dissolved in 15 ml of tetrahydrofuran (THF) under continuous magnetic stirring to form a transparent and clear homogeneous solution. Then 6 ml of deionized (DI) water was added dropwise. After stirring for 5 minutes, the as-prepared white precipitate was separated by centrifugation, washed with ethanol for several times, and dried in a vacuum at 60℃ for 12 h.

Synthesis of SnC_2O_4 nanorod-bundles: the synthetic procedure was similar to that reported for nanorod bundles, except $H_2C_2O_4$ and $SnCl_2 \cdot 2H_2O$ were first dissolved in 15 ml of dmethyl sulfoxide (DMSO).

Synthesis of SnC_2O_4 sheaf like structures: the synthetic procedure was similar with above except $H_2C_2O_4$ and $SnCl_2 \cdot 2H_2O$ were first dissolved in 15 ml of *N*-methyl-2-pyrrolidinone (NMP).

All the chemical reagents (analytical grade) were used as received without further purification. Deionized water used in all experiments. For brevity, the as-obtained samples were labeled as the sample A1, A2, and A3, respectively.

Porous SnO_2 nanostructures were obtained by annealing the as-prepared SnC_2O_4 at 350℃ at a heating rate of 2℃ min^{-1} for 2 h in air. The decomposed samples were labeled as A1-350, A2-350, and A3-350 corresponding to the calcining temperatures of 350℃.

The phase structure of the products was measured by powder X-ray diffraction (XRD) experiments on a RigaKu D/max-RB diffractometer with Ni-filtered graphite-monochromatized Cu Kα radiation (λ = 1.54056 Å). The morphology and particle sizes were observed by field emission scanning electron microcopy (FESEM, JEOL JSM-6701F). High-resolution transmission electron microscopy (HRTEM) studies were carried out on FEITECNAIF TEM (FEI, Tecnai 30) operating at an acceleration voltage of 300 kV. Samples were prepared by first dispersing the final powder in ethanol through ultrasonic treatment and the dispersion was dropped on a carbon-coated copper grid and followed by drying the samples in air for obser-

vation. The specific surface area was estimated by the Brunauer-Emmet-Teller (BET) method based on nitrogen absorption-desorption (Micromeritics ASAP 2020).The desorption isotherm was used to determine the pore size distribution via the Barret-Joyner-Halender (BJH) method. Thermogravimetric analysis (TG) of the precursor was performed on a Netzsch STA-409 PG/PC thermogravimetric analyzer (Germany). The TG curve was recorded in a dynamic atmosphere at a heating rate of 10℃ min^{-1} in the temperature range of 50∼500℃. The photoluminescence (PL) spectrum was measured at room temperature using a Xe lamp with a wavelength of 325 nm as the excitation source.

Preparation of electrodes and electrochemical measurement: the fabrication of working electrodes was carried out as follows. Briefly, the electroactive materials (SnO_2), carbon black and poly (tetrafluoroethylene) were mixed in a mass ratio of 75:20:5 and dispersed in ethanol to form a homogeneous slurry. Then the resulting mixture was pressed onto a nickel grid ($1\times1\,cm^2$) and dried at 100℃ overnight. Cyclic voltammetry (CV) measurements were done in a three-electrode cell with Pt foil ($1\times1\,cm^2$) as the counter electrode and a saturated calomel electrode (SCE) as the reference electrode. The used electrolyte was 1 M aqueous KCl solution. CV tests were employed on an electrochemical workstation (CHI 660B, Chenhua, Shanghai) between −0.6 V and −0.35 V (vs. SCE) at different scan rates of 5 and 10 mV s^{-1}.

Results and Discussion

In the present study, various SnC_2O_4 structures can be obtained by a simple precipitation process. The powder X-ray diffraction (XRD) patterns, as described in Fig. 1 shows that all the diffraction peaks are readily indexed to monoclinic tin oxalate (JCPDS Card No. 51-0614) without any impurities. The as-obtained three

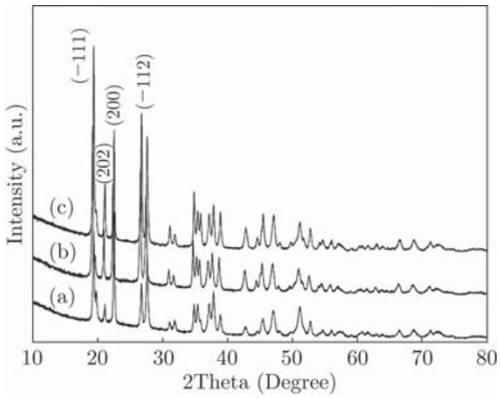

Fig. 1 XRD patterns of the as-prepared SnC_2O_4 products, (a) microfibers, (b) nanorod-bundles, and (c) sheaflike shape.

products have the similar XRD pattern indicating that the pure SnC_2O_4 product can be obtained under these experimental conditions. Moreover, the strong diffraction peaks suggest that the as-prepared samples are well crystallized.

The morphology of obtained SnC_2O_4 was first examined by FESEM. Representative FESE images are shown in Fig. 2(a)-(h). The fiber-like particles are formed with a diameter about 200∼300 nm, and lengths up to tens of micrometers with smooth surface (see Fig. 2(a) and 2(b)). When the solvent was changed to DMSO, nanorod-bundles were obtained (as shown in Fig. 2(c)). As shown in Fig. 2(d), the individual bundle comprised numerous nanorods with a diameter of about 50 nm and a length up to 20 μm. From the cross sectional image (see Fig. 2(e)), indicating that the nanorods are well-aligned despite the surface layer decorated with some nanorods in a disordered fashion. Occasionally, some well aligned nanowires-bundle can also be observed. As shown in Fig. 2(f), the well-defined nanowires-bundle with a diameter about 6 μm which was composed of a lot of closely aligned nanowires parallel to the long axis. Quite interestingly, when NMP was used as the solvent, sheaf-like product was obtained. As shown in Fig. 2(g), sheaflike particles with a bundle of filamentary crystals have been bandaged in its middle, with the top and bottom fanning out while the middle remaining thin. The individual filaments have an average diameter of 100 nm, and the sheaves are 10 μm in length. Based on the results in this study, it can be concluded that the morphology of the SnC_2O_4 was drastically influenced by the solvent. Our conclusions are based on two aspects. First, it is well-known that the intrinsic highly anisotropic bonding in the crystallographic structure plays a crucial role to direct the SnC_2O_4 with different growth patterns. SnC_2O_4 has a monoclinic lattice with three molecules per unit cell. Each Sn atom has four nearest-neighbor oxygen atoms at distances that are approximately the sum of the covalent radii and beyond these; there are three or four additional neighbors at distances that are not much larger (see Fig. 3). This structure can be thought of as made up of infinite chains of stoichiometric composition running parallel to the (101) and close to the [001] directions (see Fig. 4) [28]. Since the binding between these chains is considerably weaker than that within the chains, it suggests that cleavage may take place in the (101) planes, and preferential growth occur in the [001] direction [29]. These characteristics lead to the observed anisotropy and strong tendency to form 1-D structures. Probably, SnC_2O_4 usually exhibiting one-dimensional structures in the previous literatures are related to their strongly anisotropic crystal structure. Alivisatos and co-workers have demonstrated that the chainlike crystalline structure has a strong splitting ability [29]. In our work, the splitting structure can

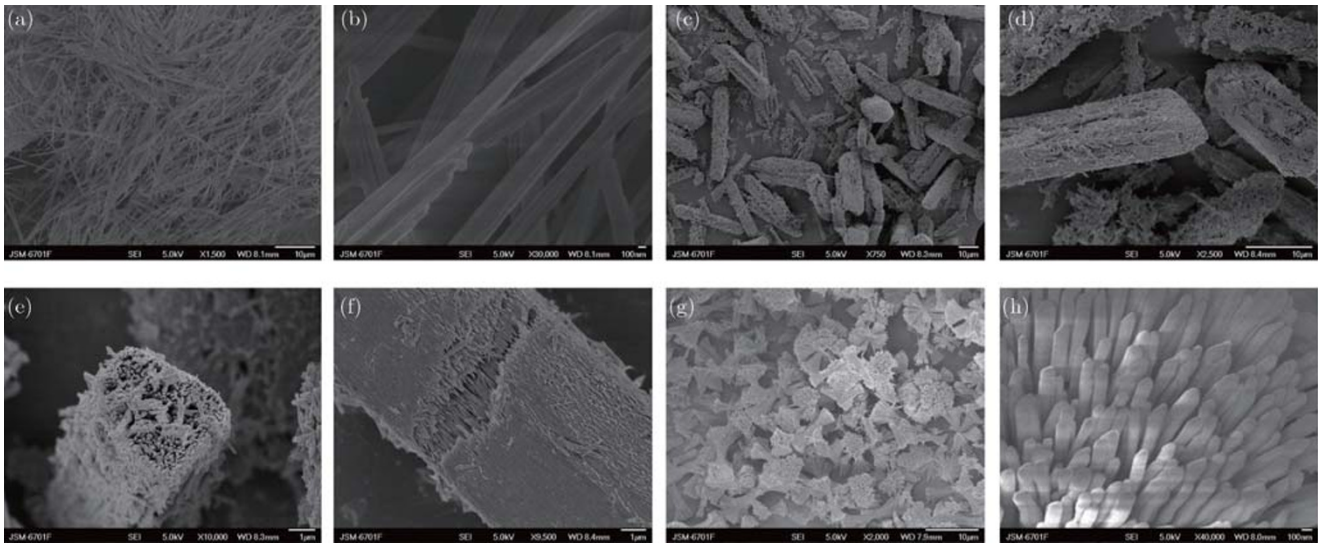

Fig. 2 FESEM images of the as-prepared SnC_2O_4 products, (a), (c), and (g) low magnification; (b), (d), and (h) high magnification; (e) cross-sectional image, (f) a well-aligned nanowires assemble bundle.

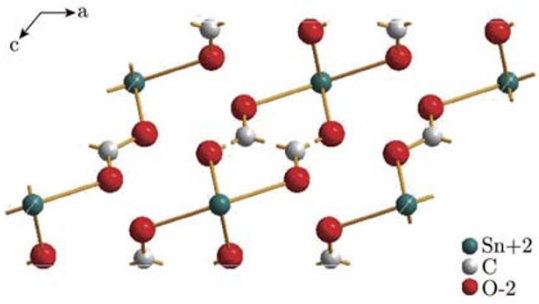

Fig. 3 The image of SnC_2O_4 crystal structure projected along [010] direction.

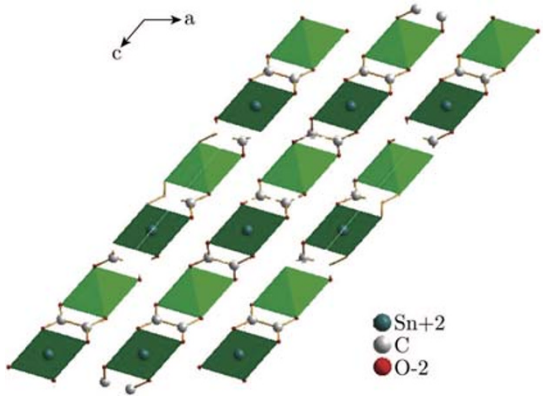

Fig. 4 The growth sequence of infinite chains viewed along the [010] direction.

only be observed in NMP. Therefore, the solvent also plays an important role to fine tuning the morphology of the product. Previous studies suggested that the variation in solubility, nucleation and growth of the resultants, reaction kinetics, solution properties, and stability of the particles in different solvent systems, leading the formation of nanostructures with different shapes [30]. Therefore, the changes of the solvents could change the nucleation and growth significantly, with which the structure of the products would change accordingly. Probably, NMP act as a surface stabilizer, which favored for crystal splitting [29]. The similar fractal growth has also been observed by Qi and co-workers, they suggested that poly (methacrylic acid) plays an important role in the fractal growth of the SrC_2O_4 aggregates, i.e. it interacts non-specifically with SrC_2O_4 crystals lead to the formation of rod-like SrC_2O_4 crystals which can act as either the rod seed or the growing rods for the successive fractal growth [31]. In our work, however, the formation of different aggregated structures is essentially in accord with their intrinsic cell structure as well as the solvent.

Previous studies demonstrate that the oxalate could be converted to the corresponding oxide via simple calcination process. Form TG curve (see Fig. 5), there was an obvious mass loss in the range of 300∼400℃, indicating they are decomposed during in this temperature range. About 34.5% weight loss is obtained and this is slightly higher than the calculated weight loss of 27.8%, which is attributed to the adsorbed water and/or solvent on the samples. The phase of the calcination product was characterized by XRD. As shown in Fig. 6, all reflection peaks can be indexed to the pure phase of SnO_2 (Cassiterite, space group: P42/mnm) with

lattice constants of a=4.73 Å, c=3.18 Å, which are consistent with the values given in the standard card (JCPDS No. 2-1340). No peaks from other phases can be detected, indicating that these architectures of SnC_2O_4 are going through complete conversion to SnO_2 after calcination at 350℃ for 2 h in air. Moreover, the XRD diffraction peaks are relatively broad, indicating a nanocrystalline nature of the product.

Representative SEM and TEM images of SnO_2 product are shown in Fig. 7∼9. From which, we can see there was no significant change the morphology of the SnC_2O_4 precursor observed, but their surfaces become coarse. As indicated in TEM data, numerous pore were formed among the primary nanoparticles due to the removal of organic species in the precursor during annealing [30]. Furthermore, the corresponding selected area electron diffraction (SAED) patterns show distinct rings: the rings from the innermost to the outside correspond to the (110), (101), (200), (211), and (310) planes of tetragonal phase of SnO_2, which are consistent with XRD result. This observation reveals that the polycrystalline nature of the as-prepared SnO_2 nanostructures. Figure 7 shows the morphological and structural characterizations of the

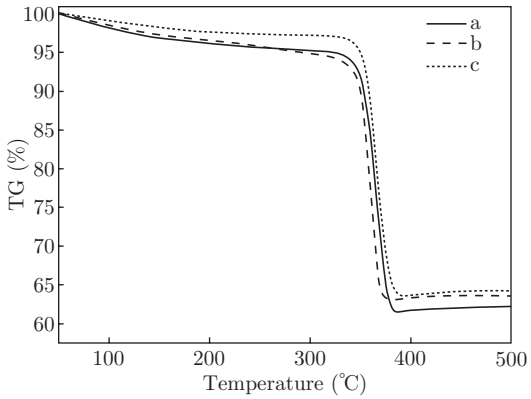

Fig. 5 Thermogravimetric analysis (TGA) curves of samples A1, A2 and A3 in air with a temperature ramp of 10℃ min^{-1}.

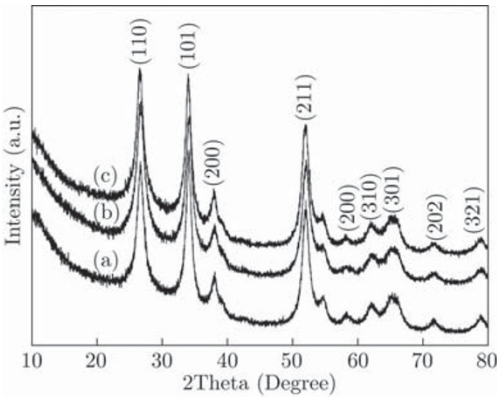

Fig. 6 XRD patterns of the products after calcination, (a) microrods, (b) nanorod-bundles, and (c) sheaflike shape.

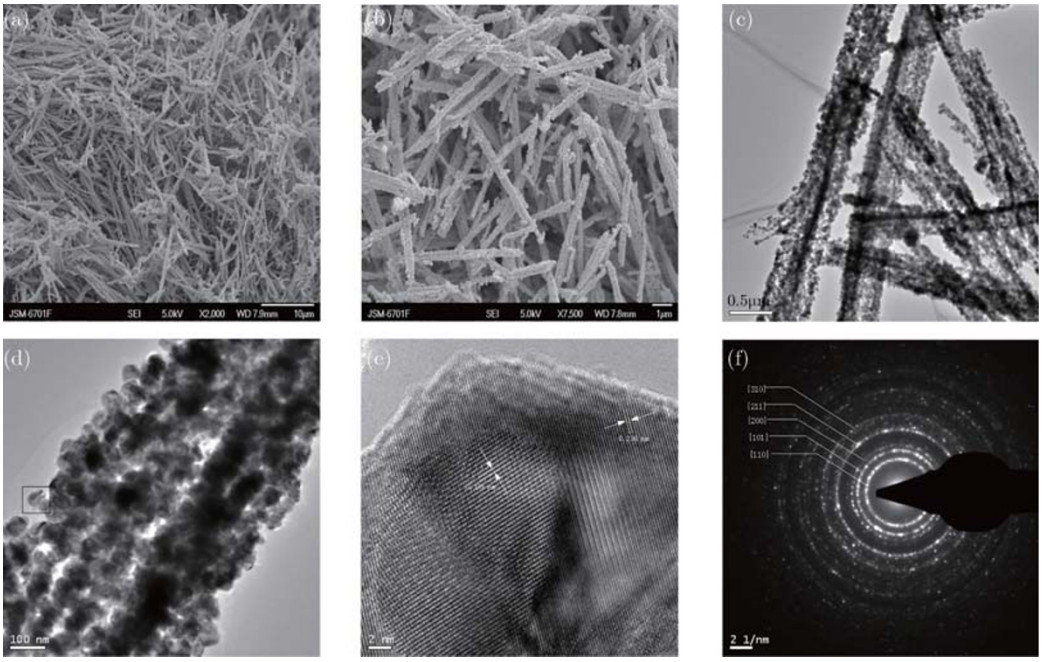

Fig. 7 FESEM and TEM images of the SnO_2 microrods (a) lower magnification, and (b) higher magnification; (c) and (d) TEM images; (e) HRTEM image, taking from the selected area marked by a square in (d). (f) the corresponding SAED pattern.

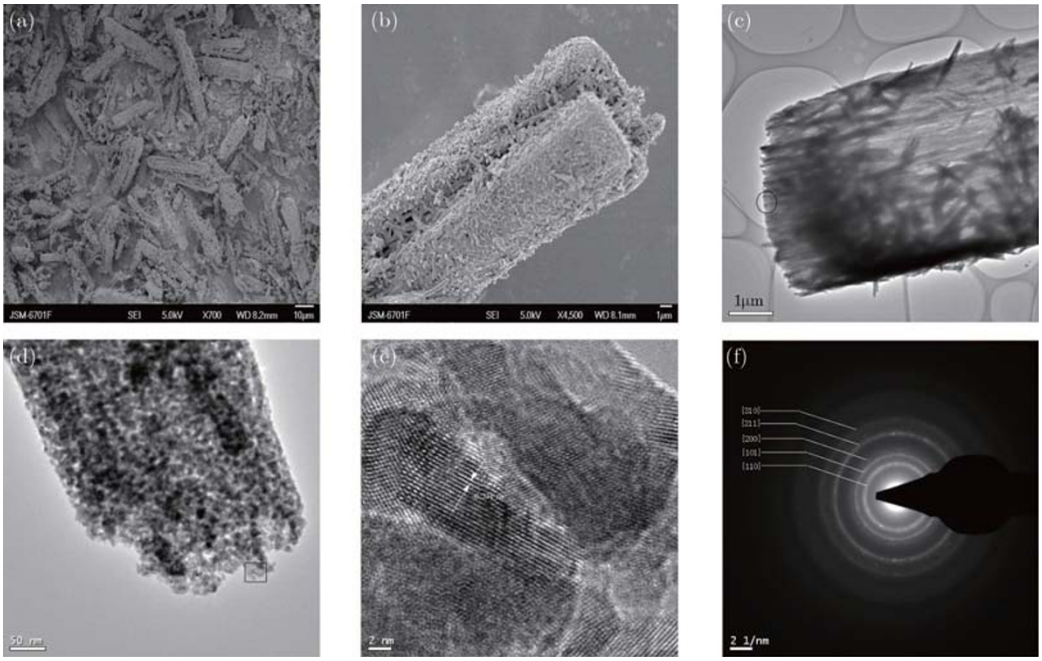

Fig. 8 FESEM and TEM images of the SnO_2 nanorod-bundles (a) lower magnification, and (b) higher magnification; (c) and (d) TEM images; The higher magnification TEM image (d) taking from the selected area marked by a circle in (c). (e) HRTEM image, taking from the selected area marked by a square in (d). (f) the corresponding SAED pattern. The fringe spacing of 0.334 nm corresponds to (110) plane of SnO_2.

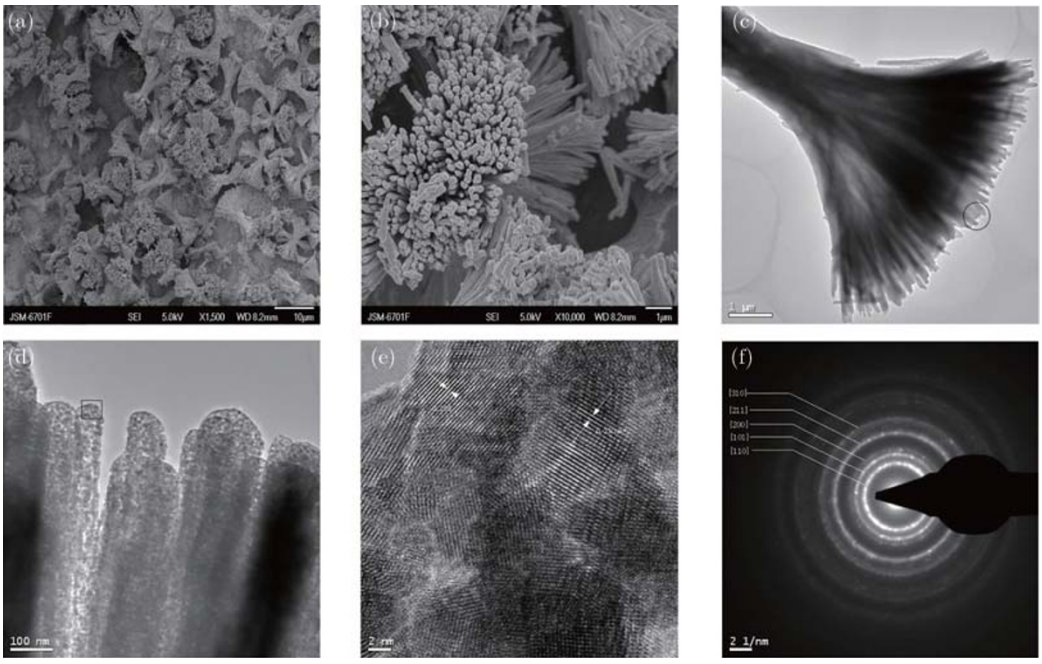

Fig. 9 FESEM and TEM images of the sheaflike shape SnO_2 (a) lower magnification, and (b) higher magnification; (c) and (d) TEM images; The higher magnification TEM image (d) taking from the selected area marked by a circle in (c). (e) HRTEM image, taking from the selected area marked by a square in (d). (f) the corresponding SAED pattern. The fringe spacing of 0.33 and 0.266 nm corresponds to (110) and (101) planes of SnO_2, respectively.

sample A1-350 prepared by the calcination of A1 at 350℃ for 2 h. From FESEM and TEM images (see Fig. 7(a)-7(c)), we can see that the whisker-like structures collapsed into porous microrods. Figure 7(d) shows the HETEM image, the fringe spacing of 0.236 and 0.333 nm corresponds to the (200) and (110) planes of SnO_2, respectively. For sample A2-350, the FESEM and TEM images, as shown in

Fig. 8, indicates that the morphology of precursor was successfully conserved as well. The nanorod-bundles with about 6 μm in diameter and tens of micrometers in length. The HRTEM image (see Fig. 8(d)) and SAED pattern (as shown Fig. 8(e)) also reveal that the product is highly crystalline. Figure 9 demonstrated that the sheaf-like nanostructures also exhibited good thermal stability and there was no substantial morphological alteration after the annealing process. From the TEM (see Fig. 9(c)) and HRTEM (see Fig. 9(d)) images, it can be observed that the sheaf-like structures are composed of porous nanorods with the diameter about 100 nm. Each nanorod composed by lots of nanoparticles, and abundant pore is formed among these nanoparticles.

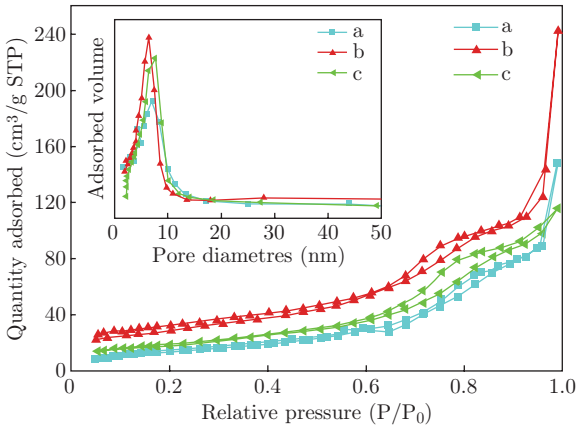

Fig. 10 N_2 adsorption–desorption isotherms of samples A1-350 (a), A2-350 (b), and A3-350 (c). The inset is the corresponding pore size distributions.

The specific surface areas of the porous SnO_2 with different shape are measured using BET method. The nitrogen physisorption isotherm exhibits a steep increase in the volume of adsorbed nitrogen, typical of pore condensation in mesoporous materials with uniform pore sizes (see Fig. 9). The BET specific surface areas of these three samples are measured to be 22.62 m^2g^{-1}, 82.67 m^2g^{-1} and 66.43 m^2g^{-1} for samples A1-350, A2-350 and A3-350, respectively. The BJH pore diameter distribution plots of the as-obtained SnO_2 products show peak at 7.15, 6.43, and 7.63 nm confirming a high degree of uniformity of the pores. Moreover, the capillary condensation step is very sharp, also indicates a narrow distribution of mesopores size. Figure 11 is the cyclic voltammetry (CV) of SnO_2 electrode in 1 M KCl at the scan rate of 5 and 10 mVs^{-1} (the voltage windows used for the three samples are from −0.6 V to −0.35 V). Figure 11 presents that all the samples show a current response like roughly rectangular mirror images with respect to the zero-current line without obvious redox peaks, which is characteristic of ideal capacitive behavior [32]. More detailed investigations are still under progress.

Figure 12 shows the PL spectra of the as-prepared SnO_2 nanostructures measured at room temperature and excited at 325 nm. The fluorescence spectra show two high-energy emission peaks at 357 and 397 nm and five weak low-energy emission peaks at 439.9, 450.6, 468.7, 483, and 492 nm. The low-energy yellow emission is believed to result from crystal defects or defect levels associated with oxygen vacancies, or tin interstitials formed during the growth. The high-energy emission cannot be assigned to the direct recombination of a conduction electron in the Sn 4p band and a hole in the O 2p valence band because of the excitation and emission are both lower than the band gap of SnO_2 sample (Eg=3.85 eV). Generally, the origin of the PL emission is mainly based on the electron transfer made by lattice defects and oxygen vacancies and the emission wavelength of the oxide material depends mainly on the particle's shape, size, and excitation wavelength [33]. The origin of the UV peak may be related to structure defects or nanocrystal grains. In the present work, the PL curves are similar for these three samples, probably resulting from the similar synthetic procedure. These as-obtained porous SnO_2 nanostructures may have a large number of defects, vacancies of oxygen, and local lattice disorder at the interface, interior and exterior surfaces.

Conclusions

In summary, well-defined SnC_2O_4 nanostructures with different morphologies were synthesized through simple solution-based direct precipitation process. The formation mechanism of such a microstructure was tentatively proposed, based on the intrinsic anisotropic crystal structure and the reaction conditions. We found that the solvent plays a vital role in determining the synthesis of

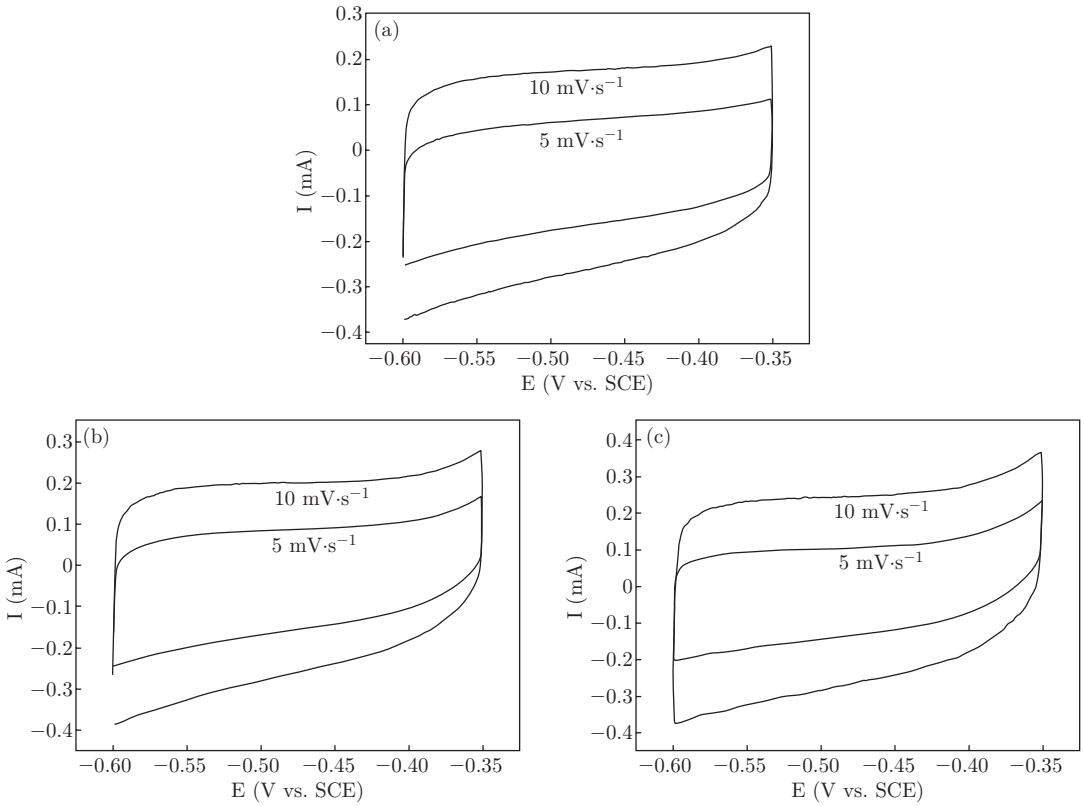

Fig. 11 Cyclic voltammograms of samples A1-350 (a), A2-350 (b), and A3-350 (c) in a 1 M KCl aqueous electrolyte at a scan rate of 5 and 10 mV s^{-1}. The voltage window used for samples are from −0.6 V to −0.35 V.

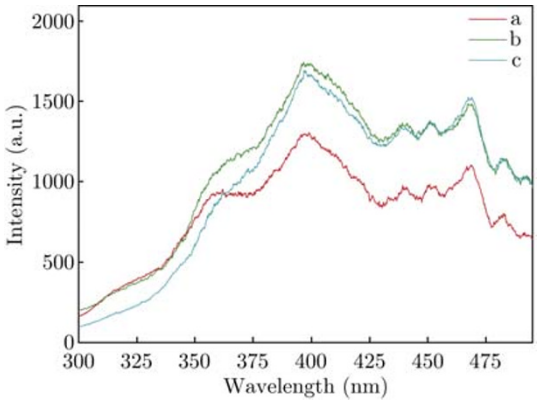

Fig. 12 Room-temperature PL spectra of samples A1-350 (a), A2-350 (b), and A3-350 (c). PL spectrum was obtained with an excitation wavelength of 325nm measured at room temperature.

SnC_2O_4 product with different shapes. After converting these three samples into pure SnO_2 by thermal annealing, the obtained porous products with high surface areas show no substantial morphological alterations. Moreover, cyclic voltammetry (CV) study shows that the shape of CV presents a current response like roughly rectangular mirror images with respect to the zero-current line without obvious redox peaks, indicating an ideal capacitive behavior of the SnO_2 electrodes. PL spectra study suggested that the as-obtained porous SnO_2 nanostructures might have a large number of defects, vacancies of oxygen, vacancy clusters and local lattice disorder at the interface, interior and exterior surfaces. This method can be easily controlled and is expected to extend to fabrication of other metal oxides with controlled shape and structure.

Acknowledgement

The authors would like to acknowledge the financial support of the National Science Foundation for Distinguished Young Scholars of China (Grant No. 51025517), the Innovative Group Foundation of NSFC (Grant No. 50721062) and the financial support of the National 973 project of China (2007CB607606).

References

[1] E. N. Dattoli, Q. Wan, W. Guo, Y. B. Chen, X. Q. Pan and W. Lu, Nano Lett. 7, 2463 (2007). http://

dx.doi.org/10.1021/nl0712217

[2] Y. Idota, T. Kubota, A. Matsufuji, Y. Maekawa and T. Miyasaka, Science 276, 1395 (1997). http://dx.doi.org/10.1126/science.276.5317.1395

[3] S. Gubbala, V. Chakrapani, V. Kumar and M. K. Sunkara, Adv. Funct. Mater. 18, 2411 (2008). http://dx.doi.org/10.1002/adfm.200800099

[4] A. Heilig, N. Barsan, U. Weimar, M. Schweizer-Berberich, J. W. Gardner and W. Gopel, Sens. Actuators B 43, 45 (1997). http://dx.doi.org/10.1016/S0925-4005(97)00096-8

[5] X. G. Han, M. S. Jin, S. F. Xie, Q. Kuang, Z. Y. Jiang, Y. Q. Jiang, Z. X. Xie and L. S. Zheng, Angew. Chem. Int. Ed. 48, 9180 (2009). http://dx.doi.org/10.1002/anie.200903926

[6] H. G. Yang and H. C. Zeng, Angew. Chem. Int. Ed. 43, 5930 (2004). http://dx.doi.org/10.1002/anie.200461129

[7] L. Vayssieres and M. Graetzel, Angew. Chem. Int. Ed. 43, 3666 (2004). http://dx.doi.org/10.1002/anie.200454000

[8] B. Cheng, J. M. Russell, W. S. Shi, L. Zhang and E. T. Samulski, J. Am. Chem. Soc. 126, 5972 (2004). http://dx.doi.org/10.1021/ja0493244

[9] M. S. Park, G. X. Wang,Y. M. Kang, D. Wexler, S. X. Dou and H. K. Liu, Angew. Chem. Int. Ed. 46, 750 (2006). http://dx.doi.org/10.1002/anie.200603309

[10] S. Mathur, S. Barth, H. Shen, J. C. Pyun and U. Werner, Small 1, 713 (2005). http://dx.doi.org/10.1002/smll.200400168

[11] M. Law, H. Kind, B. Messer, F. Kim and P. D. Yang, Angew. Chem. Int. Ed. 41, 2405 (2002). http://dx.doi.org/10.1002/1521-3773(20020703)41:13<2405::AID-ANIE2405>3.0.CO;2-3

[12] X. W. Lou, Y. Wang, C. L. Yuan, J. Y. Lee and L. A. Archer, Adv. Mater. 18, 2325 (2006). http://dx.doi.org/10.1002/adma.200600733

[13] Q. R. Zhao, Y. Gao, X. Bai, C. Z. Wu and Y. Xie, Eur. J. Inorg. Chem. 1643 (2006). http://dx.doi.org/10.1002/ejic.200500975

[14] Y. Wang, H. C. Zeng and J. Y. Lee, Adv. Mater. 18, 645 (2006). http://dx.doi.org/10.1002/adma.200501883

[15] Z. H. Wen, Q. Wang, Q. Zhang and J. H. Li, Adv. Funct. Mater. 17, 2772 (2007). http://dx.doi.org/10.1002/adfm.200600739

[16] G. J. D. Soler-illia, C. Sanchez, B. Lebeau and J. Patarin, Chem. Rev. 102, 4093 (2002). http://dx.doi.org/10.1021/cr0200062

[17] T. Waltz, B. Becker, T. Wagner, T. Sauerwald, C. D. Kohl and M. Tiemann, Sens. Actuators B 150, 788 (2010). http://dx.doi.org/10.1016/j.snb.2010.08.001

[18] J. F. Ye, H. J. Zhang, R. Yang, X. G. Li and L. M. Qi, Small 6, 296 (2010). http://dx.doi.org/10.1002/smll.200901815

[19] J. H. Ba, J. Polleux, M. Antonietti and M. Niederberger, Adv. Mater. 17, 2509 (2005). http://dx.doi.org/10.1002/adma.200501018

[20] L. Jin, L. P. Xu, C. Morein, C. H. Chen, M. Lai, S. Dharmarathna, A. Dobley and S. L. Suib, Adv. Funct. Mater. 22, 3373 (2010). http://dx.doi.org/10.1002/adfm.201001080

[21] Y. L. Wang, X. C. Jiang and Y. N. Xia, J. Am. Chem. Soc. 125, 16176 (2003). http://dx.doi.org/10.1021/ja037743f

[22] J. R. Huang, K. Yu, C. P. Gu, M. H. Zhai, Y. J. Wu, M. Yang and J. H. Liu, Sens. Actuators B 147, 467 (2010). http://dx.doi.org/10.1016/j.snb.2010.03.085

[23] C. Yu, L. Zhang, J. Shi, J. Zhao, J. Gao and D. Yan, Adv. Funct. Mater. 18, 1544 (2008). http://dx.doi.org/10.1002/adfm.200701052

[24] H. Sun, S. Z. Kang and J. Mu, Mater. Lett. 61, 4121 (2007). http://dx.doi.org/10.1016/j.matlet.2007.01.034

[25] C. K. Xu, G. D. Xu, Y. K. Liu, X. L. Zhao and G. H. Wang, Scripta Mater. 46, 789 (2002). http://dx.doi.org/10.1016/S1359-6462(02)00077-5

[26] H. Sun, S. Z. Kang and J. Mu, J. Dispersion Sci. Technol. 30, 466 (2009). http://dx.doi.org/10.1080/01932690802548916

[27] L. Y. Jiang, X. L. Wu, Y. G. Guo and L. J. Wan, J. Phys. Chem. C 113, 14213 (2009). http://dx.doi.org/10.1021/jp904209k

[28] Y. P. Fang, A. W. Xu, L. P. You, R. Q. Song, J. C. Yu, H. X. Zhang, Q. Li and H. Q. Liu, Adv. Funct. Mater. 13, 955 (2003). http://dx.doi.org/10.1002/adfm.200304470

[29] J. Tang and A. P. Alivisatos, Nano Lett. 6, 2701 (2006). http://dx.doi.org/10.1021/nl0615930

[30] D. W. Wang, Q. H. Wang, T. M. Wang, Nanotechnology 22, 135604 (2011). http://dx.doi.org/10.1088/0957-4484/22/13/135604

[31] D. B. Zhang, L. M. Qi, J. M. Ma and H. M. Cheng, Cryst. Eng. Comm. 4, 536 (2002). doi:10.1039/b207956a

[32] M. S. Wu, H. H. Hsieh, Electrochim. Acta. 53, 3427 (2008).

[33] Z. R. Dai, Z. W. Pan, Z. L. Wang, Adv. Funct. Mater. 13, 9 (2003). http://dx.doi.org/10.1002/adfm.200390013